Acta Acustica 2023, **7**, 7

https://doi.org/10.1051/aacus/2023001

Available online at:
https://acta-acustica.edpsciences.org

TECHNICAL & APPLIED ARTICLE OPEN ACCESS

Titanium ultrasonic reactor tuned to 500 kHz

Shahar Seifer*

Chemical and Biological Physics, Weizmann Institute of Science, 7610001 Rehovot, Israel

Received 15 October 2022, Accepted 18 January 2023

Abstract – This study describes the design considerations, principles, and performance of a water-filled ultrasonic reactor formed by a 125 mm size titanium cylinder covered with 67 piezoelectric transducers, tuned as a system for peak emissions at 500 kHz. The total acoustic power measured by a radiation force balance is 107 W. The sound intensity is amplified by the cavity and focusing attributes of the cylindrical wall. The reactor can generate ZnO nanoparticles from $ZnAc_2$ solution, and the nanoparticle are found fixated to an epoxy substrate as observed under a scanning transmission electron microscope. These indications are similar to a sonochemical reaction reported at 20 kHz, which validates that inertial cavitation has been reached. The titanium wall has a transmission efficiency of 51% compared to a well-matched POCO graphite-resin layer. The efficiency exceeds the value of 17% expected from a naïve calculation based on the impedance-translation theorem. The problem of optimal emission from a piezoelectric source is more complex than a simple reduction of reflections at the transducer boundary. COMSOL simulations show that the condition for optimal transmission requires consideration of elasticity and piezoelectric charge matrices instead of acoustic impedance. Approximated analytical calculation is suggested as a preliminary guidance for design of an optimal matching layer.

Keywords: Acoustic matching, Impedance-translation theorem, High-intensity ultrasound, Inertial cavitation, Nanoparticle generation, Ultrasonic reactor

1 Introduction

Acoustic matching is often ignored in everyday experience because most pressure waves that we hear originate from moving parts coupled to the target medium, such as membranes, cords, forks, or bellows. However, at high frequencies, fewer options are available to generate significant sound amplitudes. Ultrasound at frequencies above 100 kHz is generated either in piezoelectric transducers or micro-electromechanical systems, and ordinarily requires an acoustic matching layer to penetrate the medium. Reflections always exist between layers of different acoustic impedances, which facilitate the necessary resonance condition that renders significant waves. An over-simplified wave analysis may predict a full acoustic transmission between the transducer and the medium depending on constructive interference at the front end and destructive interference at the back end of the matching layer. The textbook solution to form an optimal matching layer requires certain thicknesses of $(1 + 2n)/4$ wavelength (where n is an integer number) and tuning the acoustic impedance to a value of the geometric average between the two media [1, 2]. Practically, most applications require a certain barrier in contact with the target medium, of which more affordable materials typically lack the required acoustic impedance. Work-around solutions in the form of smart materials or a stack of layers are available for acoustic matching [3, 4]. However, neglecting careful design often results in an unintended shift in the resonance frequency and consequently a compromise in performance.

This study reports on an experimental setup that has been successfully tuned to a required frequency of 500 kHz, which could not be predicted based on idealized wave analysis. The barrier layer is made of titanium with acoustic impedance of 27 MRayl, and is sandwiched between a lead zirconate titanate (PZT) piezoelectric transducer of 33 MRayl and water of 1.5 MRayl, which is far from the expected acoustic matching condition. The use of such construction to induce sonochemical reactions is also discussed.

An ultrasonic reactor is more than a simple ultrasonic bath, and offers a vast range of applications [5]. Ultrasonic baths can be used to break salts and aggregates owing to the discontinuity in the strain field caused by pressure waves. Additional effects include degassing of a liquid caused by rectified diffusion in pulsating bubbles, in which ultrasound transfers gas from the fluid to the bubbles on a cycle average [6]. To further achieve an ultrasound-induced chemical reaction, the intensity must pass a threshold to engage a state of inertial cavitation. Inertial cavitation is characterized by a violent collapse of the wall of the bubbles in liquids, during pulsation by ultrasound, which involves acceleration of the radial motion due to a feedback mechanism predicted

*Corresponding author: shahar.seifer@weizmann.ac.il

by the Rayleigh–Plesset equation. The collapse is so violent that plasma is generated at temperatures exceeding 10,000 °C for 2 ns [6]. This is useful, for example, in efficient production of biodiesel, by disturbing the phase boundary between immiscible oil and alcohol [7]. The threshold for inertial cavitation is approximately determined using a mechanical index, $\mathrm{MI} = P/f^{0.5}$, greater than 0.7 [8], where P is the amplitude of the peak rarefaction pressure in MPa and f is the frequency in Megahertz.

Sonochemical reactors are typically constructed with ultrasonic horns operating at frequencies between 20 and 40 kHz [9]. Despite higher thresholds for cavitation at higher frequencies, there are some benefits. A study demonstrated the benefit of high frequency (359 kHz) compared to low (20 kHz) in a sonochemical reaction [10], in which the former succeeds in generation of ammonia from water saturated in a nitrogen–argon mixture. Inertial cavitation based on high-frequency ultrasound can be used for the sonoporation of cell membranes [11], which serves as sterilization or a substitute for electroporation in large volumes. Moreover, small amounts of hydrogen can be produced in the presence of intensive ultrasound [12]. At intensities significantly above the cavitation threshold, such as a standing ultrasonic wave in a cavity, extreme erosion of aluminum can be achieved within seconds [13]. Sufficiently dense inertial cavitation causes rapid removal of the oxide layer and then exposes aluminum to a rapid reaction with water that releases hydrogen [14]. Therefore, the original intention of the setup was to test the feasibility of erosion in sonochemical processes; hence the reactor was designed for durability and made of titanium material. However, the erosion reaction was found to be mild at the sound intensities achieved. Nevertheless, several reactive molecules such as hydroxyl radical are formed in the collapsed bubble during inertial cavitation. The radicals in the presence of a catalyst and metal ions can form nanoparticles and throw them at high speeds at a substrate [15]. The process was found useful in production of antibacterial clothes and masks [16]; yet, the cavitation has only been tested at a relatively low frequency of 20 kHz. This study shows that nanoparticle generation and the "throwing stone" effect occur also at 500 kHz.

2 Debunking a common misconception

Designing a matching layer sandwiched between media based on the long-established impedance-translation theorem is sensible and valid in simple cases of wave propagation or acoustic analog of a transmission line [1, 2]. However, such an approach is also practiced to optimize sound emission from a piezoelectric transducer [3–17] albeit in a way that neglects the piezoelectric and elastic aspects of the layers. Moreover, the intention is to maximize the acoustic emission from the system and not just eliminate reflections at the interface between the matching layer and the transducer.

Finite element analysis is one way to show that the naive predictions are not always valid. COMSOL has been used to demonstrate the problem in a 2D simulation with a mesh size of about one-thousandth of a wavelength in the propagation direction. Figures 1a and 1c show the geometry of the setups with dimensions in meters; the color maps are predictions of a naïve wave analysis in which the former succeeds in transmission to water while the latter blocks the transmission (scale bar in dB). The blue curve in Figure 1b shows the COMSOL result of a successful 3/4-wavelength perfect matching layer (4.95 mm) for a frequency of 500 kHz in accordance with impedance-translation theorem. The PZT and matching layers are defined as liquids with appropriate density (ρ) and speed of sound (c) according to the longitudinal wave in the solids. The matching liquid layer was selected with $c = 3300$ m/s and $\rho = 2115$ kg/m^3. The incident wave is imposed on the top boundary of the top layer, and the intensity of the output acoustic emission is calculated based on the average of $P^2/\rho_w c_w$ over a volume of water (P is the total acoustic pressure and the subscript w refers to water). To prevent artifacts due to reflections, the volume of water is wrapped by additional volume similar to water but with attenuation of 1000 Np/m. The losses inside the PZT are ignored due to a lack of information but calculations show that adding losses in the PZT affects the intensity of the peak but not its frequency location. The green curves in Figures 1b and 1d show the case where the upper layer and matching layer are defined as solids with Young's modulus, Y, calculated from Lame's constants $\lambda + 2\mu$ and the Poisson ratio [18, 19]. The Poisson ratio is $\upsilon = 0.34$ according to the PZT4 that was tested. The relation to Young's modulus is $\lambda + 2\mu = Y(1-\nu)/[(1+\upsilon)(1-2\upsilon)]$, and the relation between the longitudinal speed of sound c and Lame's constants is $c = \sqrt{(\lambda+2\mu)/\rho}$, hence $Y = \rho c^2/1.539$. The calculation is based on a frequency domain solution with acoustic-structure boundary multiphysics imposed between the matching layer and the water. The orange curve (solid layers, internal source) is the more realistic case, which deviates further from the prediction of the impedance-translation theorem. The sound is generated inside the PZT layer by electric oscillations defined using the electrostatic physics module, a frequency domain solution, and the piezoelectric effect multiphysics in COMSOL. The elements of the elasticity matrix C_E (lower triangular part) are listed according to [20] $C_E = \{\lambda + 2\mu,\ \lambda,\ \lambda + 2\mu,\ \lambda,\ \lambda,\ \lambda+2\mu,\ 0,\ 0,\ 0,\ \mu, \ldots\}$, $\lambda = (\lambda + 2\mu)\upsilon/(1-\upsilon)$. The spectrum of acoustic transmission to water in the case of the orange curve in Figure 1b appears to have multiple resonances, which indicates that the resonance does not translate entirely from the transducer to the matching layer as is supposed to be in a perfect matching case. Figure 1d is calculated for the titanium barrier at a certain thickness of 6.5 mm, with the longitudinal speed of sound $c = 6070$ m/s and density $\rho = 4500$ kg/m^3. Notice that according to the blue curve in Figure 1d, a liquid layer model would not predict significant transmission via the titanium layer. However, in the model of solid layers with external source a peak of transmission occurs at 525 kHz, and for electrically excited PZT layer (orange curve) the peak transmission is found at a frequency of 494 kHz.

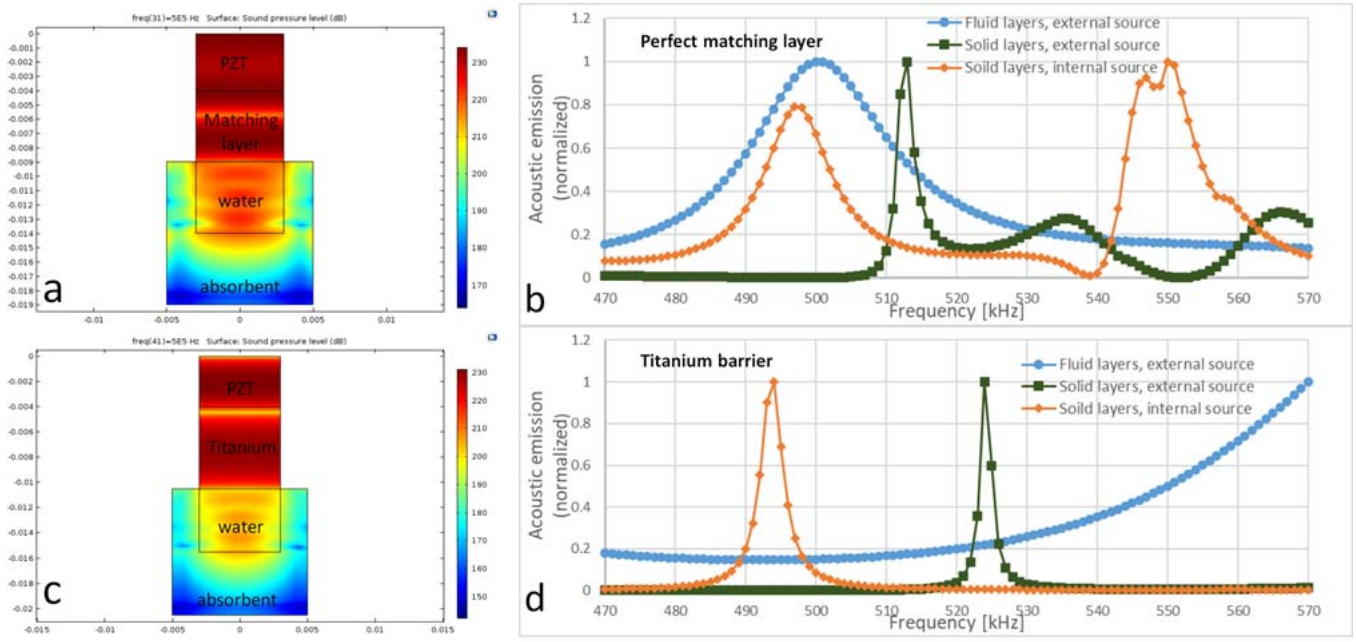

Figure 1. COMSOL finite element simulation of acoustic emission spectra in water. Blue curve – an all fluid-like layers model; green curve – a solid-like layers model (PZT and barrier) with external vibration source; orange curve – a realistic model of solid layers where the PZT is excited by electrical oscillaltions. (a) and (b) Perfect matching layer. (c) and (d) Titanium layer. Color bar – the acoustic level at 500 kHz in a naive fluid-like layer model.

The materials used in the actual experimental setup follow similar geometries and properties, except that instead of a perfectly matched layer with $\rho = 2115$ kg/m^3, the POCO material is almost perfect with $\rho = 1909$ kg/m^3. The fact that the acoustic impedance of the matching layer in the experiment is not exactly the geometrical average of the water and the PZT impedances can be ignored because a perfect match is not expected considering the complex aspects of the system.

3 Setup

The ultrasonic reactor is illustrated in Figure 2. The titanium tube (grade GR2 from Xinyi Yimao Advanced Materials Co) has an inner diameter of 125 mm, a thickness of 6.5 mm, and a total volume of 1.7 L. It is surrounded by 67 piezoelectric transducer plates ordinarily consuming an electric power of 500 W. The transducers are custom-made PZT plates made by PI Ceramics of a PIC-181 material with an active area of 46 mm × 6 mm, an acoustically optimized thickness of 4.0 mm, and a wrapped-around electrode on the side surface. The plates are glued with epoxy (RBC-3200 with A-120 hardener) using a custom jig on the titanium wall after abrading the surface with a grinding stone (Suehiro #1000). The power source is DC 72 V/12 A and the pulse triggers are controlled by a function generator (TTi, TG2000). A trigger signal of 6 V and variable frequency is fed to the first buffer stage based on P-channel and N-channel field effect transistors (FETs) in series (FQP27P06, IRF540NPBF), and then to four circuits of a high-voltage stage in a configuration of class C amplifier [21], based on a 500 V N-channel FET (STP14NM50N by ST Microelectronics) attached to a large heat sink. As discussed in [5] (Asakura, ch.5), the equivalent circuit of a piezoelectric transducer is composed of a reactive part in parallel with a mechanical impedance part, which is expected to have zero phase at the mechanical resonance. In a class C amplifier the load should be arranged as a parallel resonance circuit, which requires adding an inductor to cancel the reactance from the dielectric property of the transducer material. Thus, each group of 16-17 transducers (with a measured capacitance of 0.8 nF per transducer) is connected in parallel with eight inductors of 68 μH, also in parallel, forming an LC resonator at 500 kHz. The electrical resonator increases the voltage amplitude to 250 V pk–pk and smooths the driving current, as shown in Figure 3.

A transformer is often required to match between the electrical impedance of the transducer and that of the amplifier [5] (chap. 5). However, a detailed analysis shown by Bold [22] (Eqs. 35, 38, 69, and 71) can be used to calculate the electrical power transmission from an alternating current source of electrical impedance Z_S and voltage amplitude V_S, passing through a short cable of impedance Z_0, to a load of impedance Z_L. For a lossless cable with a length much smaller than the radio wavelength, the forward and reverse waves are added in infinite series of reflections, which results in a forward signal $V_f = 0.5\,V_S(Z_L + Z_0)/(Z_L + Z_S)$ and a reverse signal $V_r = 0.5\,V_S(Z_L - Z_0)/(Z_L + Z_S)$. The power delivered to the load is then $V_f^2/Z_0 - V_r^2/Z_0 = V_s^2 Z_L/(Z_L + Z_S)^2$. The specified impedance of the high-voltage

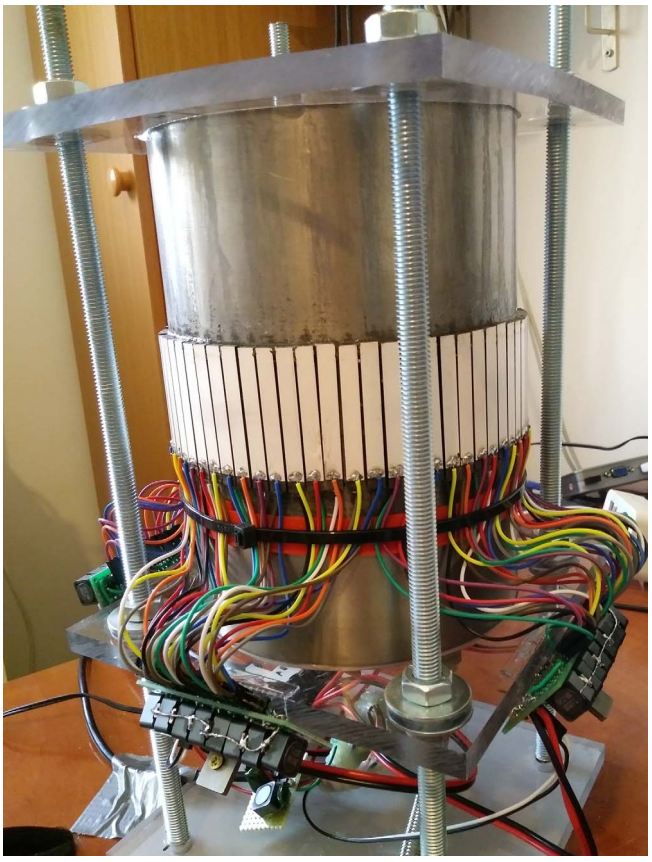

Figure 2. The ultrasonic reactor and its driving circuits.

FET in our setup during ON state is 0.4 Ω and the real part of impedance of connected 17 transducers is above 100 Ω; hence, the power delivered is nearly equal to V_S^2/Z_L regardless of the radio reflections, obviating the need for impedance matching. It is notable that a short cable of mismatched impedance has a negligible influence on the power delivery (Eq. 45 in [22]), analogous to a layer of glue that has no effect on the matching if the thickness is much smaller than the sound wavelength.

The acoustic power has been measured based on a radiation balance method described in [23] with a perfect acoustic absorber. The ponderomotive force of the acoustic waves Δm was measured with an analytical scale and converted to radiation power $\Delta\mathcal{P}$ according to $\Delta\mathcal{P} = \Delta m g c_w$, where g is the gravitational acceleration and c_w is the speed of sound in water. The radial acoustic propagation was reflected upward toward the horizontal absorber plate using an air-filled metal cone of 30°. The absorber plate was immersed in water and connected by metal frames to the scale. In another setup, the emission capacity of a single transducer was determined by gluing the PZT element to the matched layer (POCO by Entegris with impedance of 6.3 MRayl and thickness of 3/4 wavelength) which transmits maximal acoustic power to the water. The analytical scale was operated in "animal weighing" mode and the reading was scheduled at 4 s after power-up to minimize buoyancy artifacts.

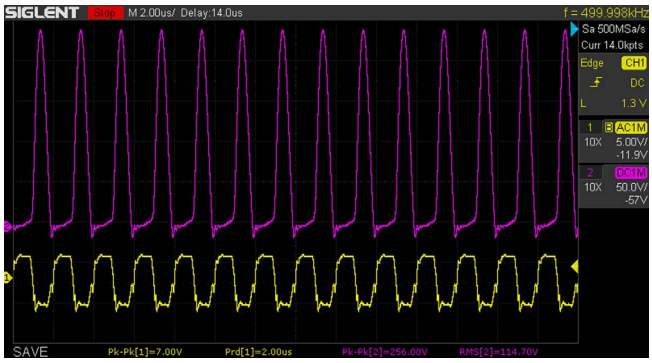

Figure 3. Oscilloscope image of the trigger signal (yellow) and the voltage applied on the piezoelectric transducers (purple) of peak-to-peak amplitude of 250 V.

4 Results

The emission of sound to water through the titanium wall is compared with the matched layer made of POCO material with 3/4-wavelength thickness. The spectrum of emission for a separate transducer with the POCO layer measured by a radiation force balance is shown in Figure 4a. The transducer is connected to the driving circuit in parallel with all other transducers of the reactor. The resonance is found at 512 kHz and the peak acoustic power is 3.1 W, meaning that 67 transducers could emit 208 W with better acoustic matching.

The total acoustic power emitted to water in the reactor is shown in Figure 4b, based on radiation force balance measurement using a conical reflector and a perfect absorber immersed in water. The values include compensation for a 16% loss due to attenuation in pure water of 0.044 np/cm/MHz [24] over a 9 cm path, and an additional 14% loss due to a 30° incidence angle at the absorber surface. The scatter of points is large due to surface waves and the violent nature of the emission. The resonance is clearly found at 500 kHz, close to the COMSOL-predicted 494 kHz, in comparison to the resonance frequency of an unloaded transducer (528 kHz based on 4.0 mm thickness and $c = 4221$ m/s in the PZT). The peak power is found at 107 W, an efficiency of 51% with respect to 208 W in the perfect matching case. The result of 51% transmission efficiency may be an underestimate because although the water was preboiled, it was not fully degassed, and along the path of 9 cm from the wall to the absorber the sound may be scattered. However, the result is much higher than a naïve calculation of the transmission efficiency following [1] based on acoustic impedances Z_i for the longitudinal waves (in PZT, titanium and water), the thickness of the middle layer t_2, and the wavelength k_2 at 500 kHz, expecting transmission ratio of $I_3/I_1 = 4Z_1Z_3/\{(Z_3 + Z_1)^2\cos^2(k_2t_2) + (Z_2 + Z_1Z_3/Z_2)^2\sin^2(k_2t_2)\} = 17\%$.

The power consumption is measured on the mains power line as a function of the trigger frequency, with the peak in power consumption being 560 W at 503 kHz according to Figure 4c, which strengthens confidence in the location of the resonance frequency. Based on the lumped electrical

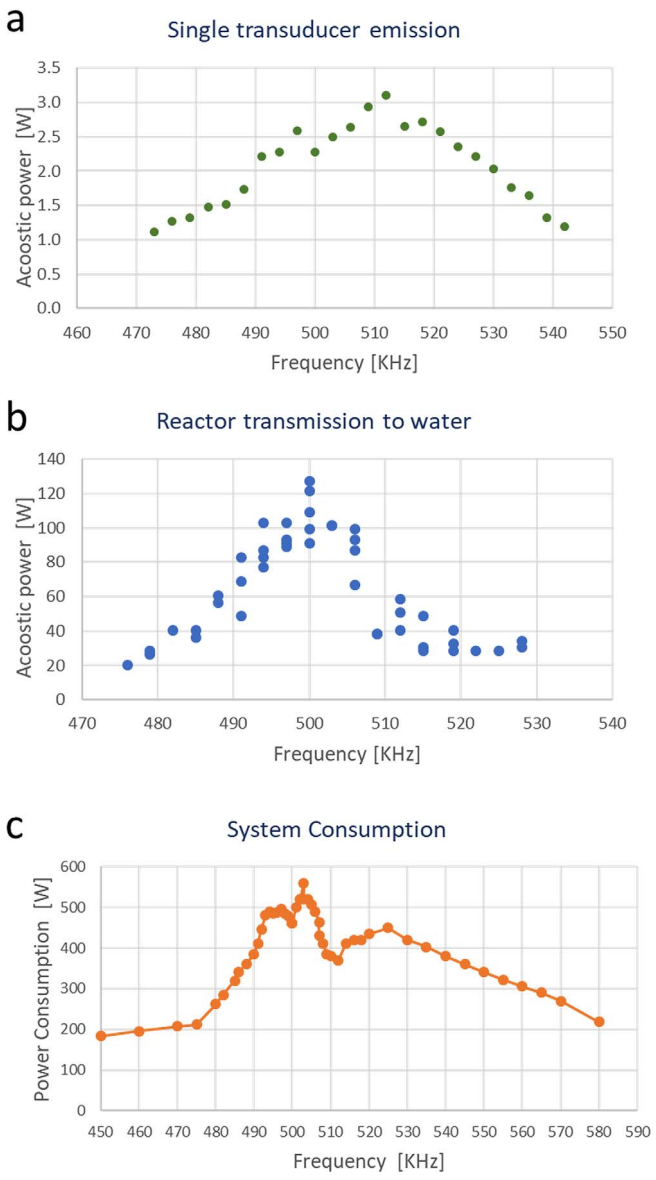

Figure 4. Power spectra. (a) Acoustic power emission from a single transducer element with POCO matching layer, with a peak of 3.1 W at 512 kHz. (b) Acoustic power measured inside the reactor, with an average peak of 107 W at 500 kHz. (c) Electrical power consumption of the reactor, with a peak of 560 W at 503 kHz.

circuit of the piezoelectric transducer [5, 25], the mechanical resonance frequency is very close to the point of minimum electrical impedance, in which the power consumption is maximal. To understand how much of the energy consumption is dissipated by the transducers, the rate of temperature change in water has been measured using a thermocouple. The temperature rise is 15 °C in 8 min during sonication, and the cooling rate is 2.4 °C in 8 min. Based on these values and the heat capacity of water, the power consumed by the transducers is approximately 290 W, and the remainder is dissipated in the circuit (the 4 power transistors include large heat sinks cooled by a fan). Hence, the electromechanical efficiency of the PZT and wall combined can be calculated as $107/(107 + 290) = 27\%$, whereas the specified electromechanical efficiency of PIC181 PZT is 46%, and the maximum reported for capacitive micromachined ultrasound transducers (CMUT) is 95% [26]. Yet, the peak frequency of titanium CMUT that has been produced so far stands at 3 kHz [27].

The curvature of the cylindrical wall causes beam convergence at the center, presumably to a spot of three wavelengths size. So the amplification in sound intensity is expected to be a factor of [cylinder diameter]/[3 wavelengths] = 14. Furthermore, about 80% of the power is reflected at the inner side of the wall, which introduces a cavity gain. Taking into account the attenuation in water after one pass from the center to the wall and back, the returning power by a single reflection is about 50%. A geometric series of residual reflections of 50% contributes an additional intensity amplification factor of 2. Hence the effective acoustic intensity at the center is higher than the one estimated near the wall. Based on the measured acoustic power of 107 W amplified by 2, and focused by a factor of 14, the expected intensity is $I = 14 \times 2 \times 107$ W/200 cm^2 = 15 W/cm^2. Using $I = P^2/2Z$, where Z is the acoustic impedance of water, the mechanical index is calculated as MI = 0.9; therefore, inertial cavitation can be reached because it is above the required value of 0.7.

By filling non-degassed water in the reactor, bubbles form during the ultrasound emission. However, after 8 min of sonication and the temperature reaching 50 °C, the water appears completely degassed; thus, the attenuation is minimal. An effect indicating the condition of fully degassed water being achieved is the emergence of surface waves on the water surface, as shown in Figure 5a.

The reactor has been tested for sonochemical reaction of aluminum and water using an aluminum disc placed in water and rotated at 1800 RPM during sonication. Traces of hydrogen have been detected using a properly-warmed hydrogen detector (Winson, MQ-8). The hydrogen detection response occurs only when active sonication is combined with the plate rotation (sensor voltage increased from 0.46 to 0.64 V), which indicates traces of hydrogen emission at low concentrations, starting from 100 ppm.

The ultrasonic reactor has been tested for generation of ZnO nanoparticles, following the protocol in [16]. The solution contained zinc acetate 0.01 Molar in deionized water. The solution was degassed and heated by the power emitted from the transducers, while the excitation frequency was adjusted by 0.06 kHz/°C to achieve maximum power consumption, based on feedback of the power meter. At a temperature of 68 °C a concentrated solution of Ammonium Hydroxide was added (0.02 Molar in the final solution) to serve as a catalyst. Immediately after, a piece of epoxy rod was immersed in the sonicated solution for one minute. XRD analysis indicated the presence of hexagonal ZnO crystals in the dry precipitation material [28]. A vertical cut from the surface of the cylindrical epoxy rod was placed in a scanning transmission electron microscope, configured as described in [29] with a high angle dark field detector. Two scans were acquired at a thin area of the specimen with a difference of 40° in the tilt angle, shown

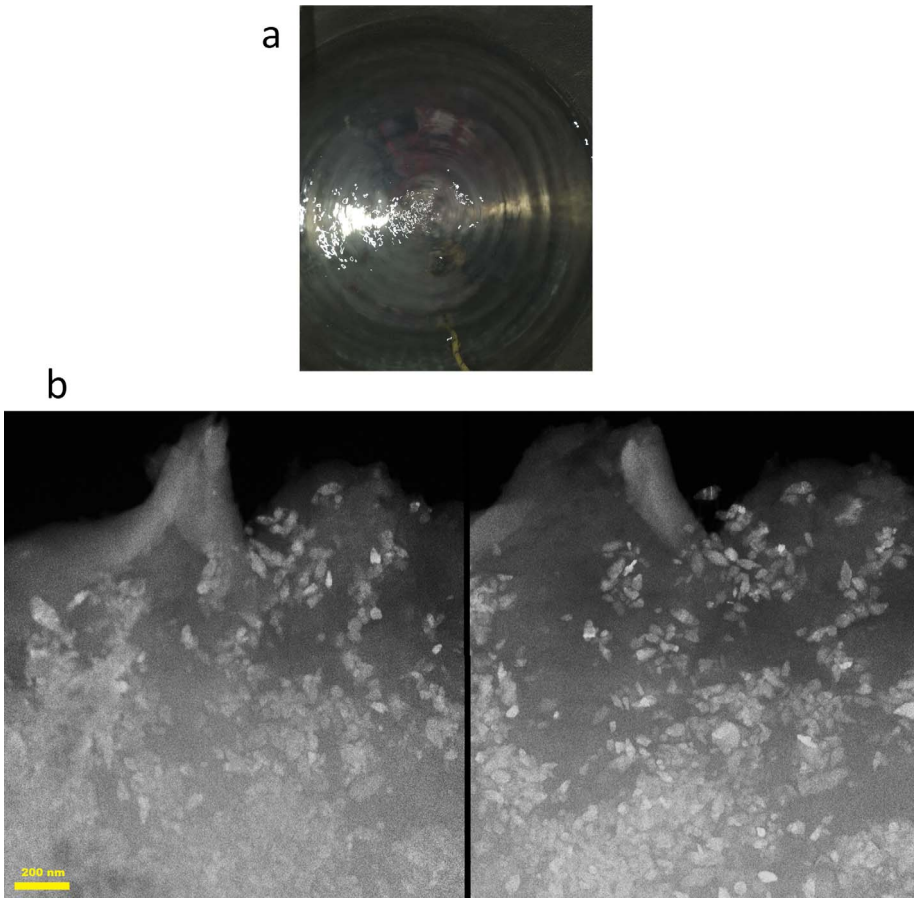

Figure 5. (a) Surface waves appear after the water is fully degassed. (b) Stereoscopic view of ZnO nanoparticles found embedded in an epoxy substrate after sonication (images from a scanning transmission electron microscope).

in Figure 5b as a stereoscopic view. According to the 3D view, the nanoparticles are multi-depth distributed inside the epoxy, in agreement with the theory that inertial cavitation causes penetration of the nanoparticles to a substrate by a "throwing stones" mechanism [16]. The specimen is not uniformly distributed with nanoparticles, in contrast to the results achieved at lower sonication frequency with enzymatic pretreatment [30]. The aspect ratio of the rapidly formed nanoparticles is low in comparison to a 90 min sol–gel process that forms disk-shaped nanocrystals of 4 µm diameter [31]. The generation of the nanoparticles is attributed to the generation of hydroxyl radicals in the plasma of the collapsing bubbles during inertial cavitation [6, 16].

5 Practical transmission model for piezoelectric source

To facilitate an easier design of a matching layer with consideration of piezoelectric sound source in the first layer, a reduced analytical calculation may be used as a preliminary estimate. The calculation ignores the finite width of the transducer and the non-longitudinal vibration modes. The resonant peak is calculated for a system of a piezoelectric material, a barrier that is called a spring-mass damper (SMD [32]), a water front and air backing. An example is a PZT plate of thickness t_{pzt} glued to a titanium plate (curvature neglected) of thickness t_{smd} in contact with water. The backing of the PZT is air. The propagation direction is normal to the plane of interfaces and all transverse aspects and dissipation influences are ignored. The polycrystalline nature of the PZT supports partly such an assumption in actual plates. Following the treatment in [32] we assume that the electric field, E_3, is uniform across the PZT and therefore relates to the oscillatory voltage according to

$$E_3 = \mathrm{Voltage}/t_{\mathrm{pzt}}. \tag{1}$$

Other notations follow the IEEE standard of piezoelectricity [33] except for denoting k_{pzt}, k_{smd}, and k_w as the wavenumber in PZT, titanium, and water, respectively. The wavenumber is proportional to the angular frequency of sound, ω, according to the usual dispersion relation $k = \omega/c$.

The displacement amplitudes of the forward and reverse waves are denoted as A and B for PZT, C and D for titanium, and E for the emitted wave in water. The five unknown parameters A, B, C, D, and E can be solved using the following boundary conditions:

Table 1. Properties included in the calculation.

Variable	Value	Description
Voltage	35 [volt]	Amplitude of excitation voltage
d_{33}	265e−12 [C/N]	PZT piezoelectric charge constant (PIC181)
ε_{33}	1200 × 8.85e−12	PZT permittivity (PIC 181)
t_{smd}	6.5e−3 [m]	Thickness of titanium wall
c_{pzt}	4221 [m/s]	Longitudinal speed of sound in PZT4
c_w	1480 [m/s]	Speed of sound in water
c_{smd}	6070 [m/s]	Speed of sound in titanium (Engineering Toolbox)
ρ_{smd}	4500 [kg/m^3]	Titanium density
ρ_w	1000 [kg/m^3]	Water density
ρ_{pzt}	7800 [kg/m^3]	PZT density (PIC 181)
ν_{pzt}	0.34	Poisson ratio (PIC 181)
Y_{smd}	102.7e9 [Pa]	Young's modulus of titanium GR2 (AmesWeb)
A_S	1e−4 [m^2]	Area of transducer

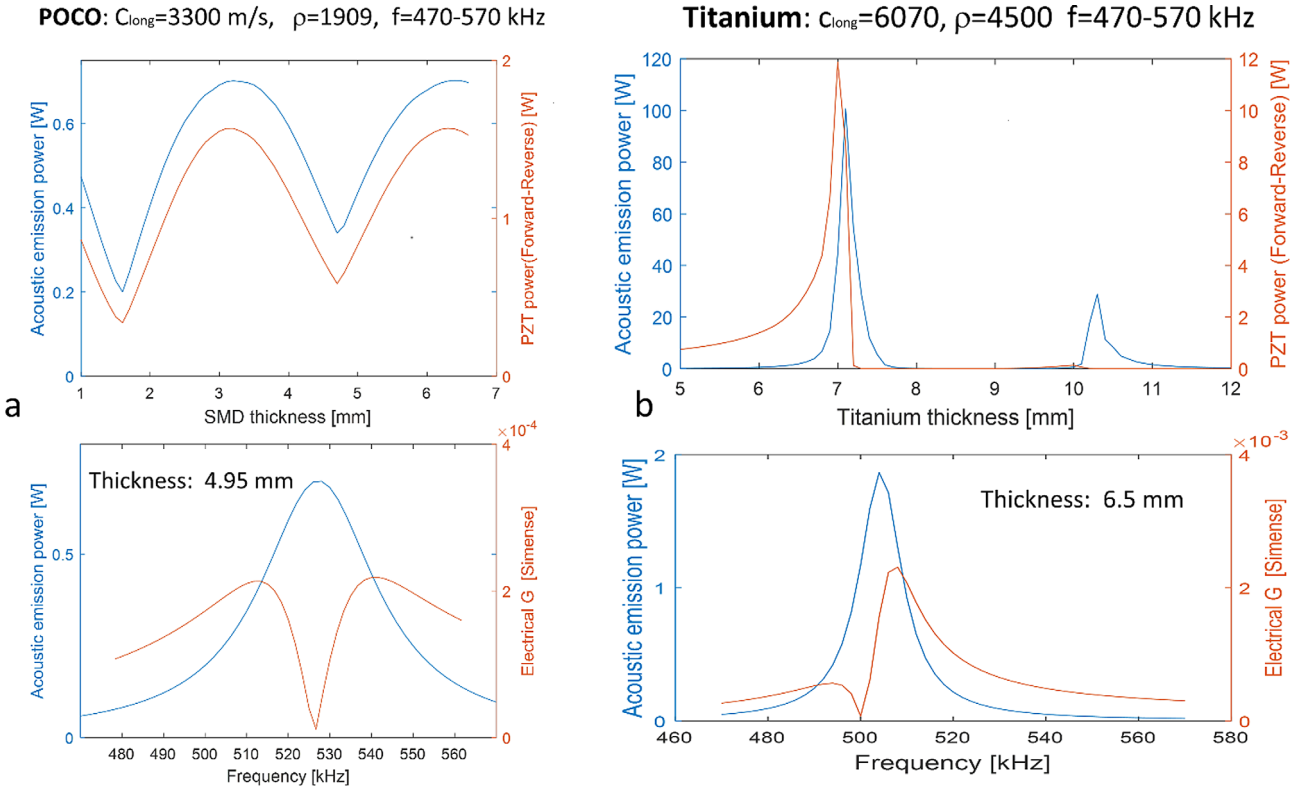

Figure 6. Calculations based on the proposed analytical formulas. In the top plots, the maximum acoustic emission is shown as a function of the matching-layer thickness, with frequency tolerance between 470–570 kHz. The bottom plots show the acoustic emission as a function of the frequency of PZT excitation, at the thicknesses chosen in the experiment. (a) POCO matching layer. (b) Titanium matching layer.

1. Zero stress on the boundary with air.
2. Continuity of displacement at the boundary between PZT and titanium.
3. Continuity of stress at the boundary between PZT and titanium.
4. Continuity of stress at the boundary between titanium and water.
5. Continuity of displacement at the boundary between titanium and water.

After determining the displacement amplitude E (dependent on the voltage amplitude), the acoustic power in water is calculated as follows:

$$\text{Acoustic power} = \frac{1}{2} A_S \rho_w c_w \omega^2 E^2, \tag{2}$$

where A_S is the transducer surface area and c_w is the speed of sound in water. In the case of isotropic materials, an additional parameter for each solid material is the Young's

modulus Y, which is reciprocally related to the 3rd diagonal element in the elastic compliance matrix [20]. In water the bulk modulus is denoted K_w. The set of equations related to the boundary conditions is expressed as follows (excluding time variation):

$$I = i\omega A_3 D_3 = i\omega A_S\left(\varepsilon_{33}^T E_3 + d_{33} T_3\right), \tag{3}$$

$$d_{33}E_3 = S_3 = \frac{\partial u_3}{\partial x_3}(x_3 = 0) = -ik_{\mathrm{pzt}}A + ik_{\mathrm{pzt}}B, \tag{4}$$

$$Ae^{-ik_{\mathrm{pzt}}t_{\mathrm{pzt}}} + Be^{ik_{\mathrm{pzt}}t_{\mathrm{pzt}}} = Ce^{-ik_{\mathrm{smd}}t_{\mathrm{pzt}}} + De^{ik_{\mathrm{smd}}t_{\mathrm{pzt}}}, \tag{5}$$

$$\begin{aligned} &Y_{\mathrm{pzt}}\left(-ik_{\mathrm{pzt}}Ae^{-ik_{\mathrm{pzt}}t_{\mathrm{pzt}}} + ik_{\mathrm{pzt}}Be^{ik_{\mathrm{pzt}}t_{\mathrm{pzt}}} - d_{33}E_3\right) \\ &\quad = Y_{\mathrm{smd}}\left(-ik_{\mathrm{smd}}Ce^{-ik_{\mathrm{smd}}t_{\mathrm{pzt}}} + ik_{\mathrm{smd}}De^{ik_{\mathrm{smd}}t_{\mathrm{pzt}}}\right), \end{aligned} \tag{6}$$

$$\begin{aligned} &Y_{\mathrm{smd}}\left(-ik_{\mathrm{smd}}Ce^{-ik_{\mathrm{smd}}(t_{\mathrm{pzt}}+t_{\mathrm{smd}})} + ik_{\mathrm{smd}}De^{ik_{\mathrm{smd}}(t_{\mathrm{pzt}}+t_{\mathrm{smd}})}\right) \\ &\quad = K_w\left(-ik_w Ee^{-ik_w(t_{\mathrm{pzt}}+t_{\mathrm{smd}})}\right), \end{aligned} \tag{7}$$

$$Ce^{-ik_{\mathrm{smd}}(t_{\mathrm{pzt}}+t_{\mathrm{smd}})} + De^{ik_{\mathrm{smd}}(t_{\mathrm{pzt}}+t_{\mathrm{smd}})}) = Ee^{-ik_w(t_{pzt}+t_{smd})}. \tag{8}$$

Hence, the acoustic power transmitted to water is determined by several parameters such as the voltage amplitude, the excitation frequency, the thickness of the PZT, the properties of the PZT, and the thickness of the titanium layer. The calculation script is written in MATLAB (available in the repository [28]) and refers to the parameters listed in Table 1. First, the PZT thickness is determined based on the requested resonance frequency of around 500 kHz according to the manufacturer's tables. Thereafter, the best SMD thickness is determined as shown in the top plots in Figure 6. In the next step, we set the PZT thickness and the SMD thickness and find the emission spectrum versus frequency, then iterate the analysis until the requested resonance location is reached as shown in the bottom plots of Figure 6. With a titanium thickness of 6.5 mm and PZT thickness of 4.0 mm (Fig. 6b), the resonance is determined to be slightly above 500 kHz and the minimum admittance exactly at 500 kHz. However, with a slightly thicker titanium layer the emission is predicted to increase, provided that a tolerance of frequencies is allowed between 470 and 570 kHz. Similarly, for the POCO material (Fig. 6a) the expected resonance is found at 525 kHz while experimentally it was found at 512 kHz. According to the calculation, a 6 mm POCO layer may achieve as much as twice the measured transmission with a 3/4-wavelength layer thickness.

6 Conclusions

From analysis of the stress, strain, electric displacement field, and the elastic and piezoelectric properties of the solid layers, acoustic radiation can be transmitted efficiently to water even across a titanium barrier. The titanium layer compared with a perfect matching layer is at least 51% efficient in transmission. The total acoustic power of the reactor is approximately 110 W, and, owing to amplification induced by cavity and focusing effects, the mechanical index is estimated above the threshold of inertial cavitation. The intensity is insufficient to induce significant erosion in aluminum, but nonetheless, sonochemical reactions occur and ZnO nanoparticles can be generated. The peak acoustic power in water is found at a frequency of 500 kHz, close to the predicted value of 494 kHz according to COMSOL simulation and 505 kHz according to an approximated analytical calculation. The calculation can be used as an estimate in design before applying a detailed simulation of finite element analysis.

Conflict of interest

The authors declare no conflict of interest.

Acknowledgments

The author is grateful to Aharon Gedanken and Nina Perkas from Bar-Ilan University for hosting and setting up the first experiment for generation of nanoparticles.

Data availability statement

All data that support the findings of this study are included within the article.

References

1. L.E. Kinsler: *Fundamentals of acoustics*, 3rd ed., Wiley, New York, 1982.
2. B.E. Anderson, S.D. Sommerfeldt: Solving one-dimensional acoustic systems using the impedance translation theorem and equivalent circuits: a graduate level homework assignment. *The Journal of the Acoustical Society of America* 150 (2021) 4155. https://doi.org/10.1121/10.0008932.
3. V.T. Rathod: A review of acoustic impedance matching techniques for piezoelectric sensors and transducers. Sensors 20 (2020) 4051. https://doi.org/10.3390/s20144051.
4. R. Hill, S.M.A. El-Dardiry: A theory for optimization in the use of acoustic emission transducers. *The Journal of the Acoustical Society of America* 67 (1980) 673–682. https://doi.org/10.1121/1.383893.
5. F. Grieser, P.K. Choi, N. Enomoto, H. Harada, K. Okitsu, K. Yasui: *Sonochemistry and the acoustic bubble*, Elsevier, 2015.
6. K. Yasui: *Acoustic cavitation and bubble dynamics*, Springer, 2018.
7. A.D. Patil, S.S. Baral, P.B. Dhanke, C.S. Madankar, U.S. Patil, V.S. Kore: Parametric studies of methyl esters synthesis from Thumba seed oil using heterogeneous catalyst under conventional stirring and ultrasonic cavitation. *Materials Science for Energy Technologies* 1 (2018) 106–116. https://doi.org/10.1016/j.mset.2018.06.004.
8. R.E. Apfel, C.K. Holland: Gauging the likelihood of cavitation from short-pulse, low-duty cycle diagnostic ultrasound. *Ultrasound in Medicine & Biology* 17 (1991) 179–185. https://doi.org/10.1016/0301-5629(91)90125-G.

9. P.R. Gogate, P.A. Tatake, P.M. Kanthale, A.B. Pandit: Mapping of sonochemical reactors: Review, analysis, and experimental verification. *AIChE Journal* 48 (2002) 1542–1560. https://doi.org/10.1002/aic.690480717.
10. T. Ouerhani, R. Pflieger, W. Ben Messaoud, S.I. Nikitenko: Spectroscopy of sonoluminescence and sonochemistry in water saturated with N_2–Ar mixtures. The Journal of Physical Chemistry B 119 (2015) 15885–15891. https://doi.org/10.1021/acs.jpcb.5b10221.
11. G.H. Kelsall, S. Tang, S. Yurdakul, A.L. Smith: Electrophoretic behaviour of bubbles in aqueous electrolytes. *Journal of the Chemical Society, Faraday Transactions* 92 (1996) 3887–3893. https://doi.org/10.1039/FT9969203887.
12. M. Penconi, F. Rossi, F. Ortica, F. Elisei, P.L. Gentili: Hydrogen production from water by photolysis, sonolysis and sonophotolysis with solid solutions of rare earth, gallium and indium oxides as heterogeneous catalysts. *Sustainability* 7 (2015) 9310–9325. https://doi.org/10.3390/su7079310.
13. O. Johansson, T. Pamidi, T. Lofqvist: Design of a high-intensity ultrasound reactor, The Institute of Electrical and Electronics Engineers, Inc., IEEE, Piscataway. 2017, p. 1.
14. J. Petrovic, G. Thomas: Reaction of aluminum with water to produce hydrogen, 2008, p. 26.
15. A. Gedanken, N. Perkas: in: M. Rizzo, G. Bruno, Eds. *Surface coatings*, Hauppauge, United states: Nova Science Publishers, Incorporated, 2009:213–236.
16. I. Perelshtein, N. Perkas, A. Gedanken: 12 – the sonochemical coating of textiles with antibacterial nanoparticles, in: A. Tiwari, Ed. *Handbook of antimicrobial coatings*, Elsevier, 2018:235–255. https://doi.org/10.1016/B978-0-12-811982-2.00012-3.
17. H.W. Persson, C.H. Hertz, Acoustic impedance matching of medical ultrasound transducers, *Ultrasonics* 23 (1985) 83–89. https://doi.org/10.1016/0041-624X(85)90037-X.
18. R. Truell, C. Elbaum, B.B. Chick: 1 – propagation of stress waves in solids, in: R. Truell, C. Elbaum, B.B. Chick, Eds. *Ultrasonic methods in solid state physics*, Academic Press, 1969:1–52. https://doi.org/10.1016/B978-1-4832-3318-5.50006-7.
19. H. Azhari: Basics of biomedical ultrasound for engineers, Wiley, Wiley.com, 2010. https://www.wiley.com/en-gb/Basics+of+Biomedical+Ultrasound+for+Engineers-p-9780470465479.
20. COMSOL documentation – ver. 5.4, 2019. COMSOL Inc. https://doc.comsol.com/5.4/doc/com.comsol.help.sme/sme_ug_theory.06.23.html.
21. W. Storr: Amplifier classes and the classification of amplifiers, Basic Electronics Tutorials, 2013 (accessed January 4, 2023). https://www.electronics-tutorials.ws/amplifier/amplifier-classes.html
22. G. Bold: The Bruene directional coupler and transmission lines, 2009. https://www.collinsradio.org. https://www.collinsradio.org/wp-content/uploads/2015/05/Understanding-the-Bruene-Coupler-Transmission-Line-Bold.pdf
23. Y. Sutton, A. Shaw, B. Zeqiri: Measurement of ultrasonic power using an acoustically absorbing well. *Ultrasound in Medicine & Biology* 29 (2003) 1507–1513. https://doi.org/10.1016/S0301-5629(03)01036-6.
24. R. Martinez, L. Leija, A. Vera: Ultrasonic attenuation in pure water: Comparison between through-transmission and pulse-echo techniques. In: 2010 Pan American health care exchanges, 15–19 March 2010, Lima, Peru, pp. 81–84. https://doi.org/10.1109/PAHCE.2010.5474593.
25. E. Hafner: The piezoelectric crystal unit – Definitions and methods of measurement. Proceedings of the IEEE, 57 (1969) 179–201. https://doi.org/10.1109/PROC.1969.6912.
26. E.B. Dew, A. Kashani Ilkhechi, M. Maadi, N.J.M. Haven, R.J. Zemp: Outperforming piezoelectric ultrasonics with high-reliability single-membrane CMUT array elements. *Microsystems & Nanoengineering* 8 (2022) 1–15. https://doi.org/10.1038/s41378-022-00392-0.
27. L. Prochazka, A. Huber, M. Schneider, N. Ghafoor, J. Birch, F. Pfiffner: Novel fabrication technology for clamped micron-thick titanium diaphragms used for the packaging of an implantable MEMS acoustic transducer. *Micromachines* 13 (2021) 74. https://doi.org/10.3390/mi13010074.
28. S. Seifer, N. Perkas: [Data set]. GitHub. https://github.com/Pr4Et/Supplementaries/tree/main/SMD_matching.
29. S. Seifer, L. Houben, M. Elbaum: Flexible STEM with simultaneous phase and depth contrast. *Microscopy and Microanalysis* 27 (2021) 1476–1487. https://doi.org/10.1017/S1431927621012861.
30. I. Perelshtein, Y. Ruderman, N. Perkas, K. Traeger, T. Tzanov, J. Beddow, E. Joyce, T.J. Mason, M. Blanes, K. Mollá, A. Gedanken: Enzymatic pre-treatment as a means of enhancing the antibacterial activity and stability of ZnO nanoparticles sonochemically coated on cotton fabrics. Journal of Materials Chemistry 22 (2012) 10736–10742. https://doi.org/10.1039/C2JM31054F.
31. M.T. Thein, S.-Y. Pung, A. Aziz, M. Itoh: The role of ammonia hydroxide in the formation of ZnO hexagonal nanodisks using sol–gel technique and their photocatalytic study. Journal of Experimental Nanoscience 10 (2015) 1068–1081. https://doi.org/10.1080/17458080.2014.953609.
32. C. Liang, F.P. Sun, C.A. Rogers: Coupled electro-mechanical analysis of adaptive material systems – determination of the actuator power consumption and system energy transfer. Journal of Intelligent Material Systems and Structures 5 (1994) 12–20. https://doi.org/10.1177/1045389X9400500102.
33. IEEE Standard on Piezoelectricity: ANSI/IEEE Std 176-1987, 1988, p. 0_1. https://doi.org/10.1109/IEEESTD.1988.79638.

Cite this article as: Seifer S. 2023. Titanium ultrasonic reactor tuned to 500 kHz. Acta Acustica, **7**, 7.